PAPER • **OPEN ACCESS**

Synthesis, characterization and antiviral efficacy of valacyclovir loaded polymeric nanoparticles against wild-type herpes simplex virus type 2

To cite this article: Oluwafemi Samuel Obisesan *et al* 2025 *Biomed. Mater.* **20** 045014

IOP Publishing Biomed. Mater. 20 (2025) 045014 https://doi.org/10.1088/1748-605X/addf25

Biomedical Materials

OPEN ACCESS

RECEIVED
30 September 2024

REVISED
8 May 2025

ACCEPTED FOR PUBLICATION
30 May 2025

PUBLISHED
10 June 2025

PAPER

Synthesis, characterization and antiviral efficacy of valacyclovir loaded polymeric nanoparticles against wild-type herpes simplex virus type 2

Oluwafemi Samuel Obisesan[1,4,*], Lesego Tshweu[2,6], Lindiwe Nkabinde-Thete[3], Bathabile Ramalapa[2,6], Mpho Phehello Ngoepe[1], Roux Saartjie[1,5] and Hazel Tumelo Mufhandu[1]

[1] DSI-Mandela Nanomedicine Platform, Nelson Mandela University, Gqeberha 6001, Eastern Cape, South Africa
[2] Biotherapeutics Delivery laboratory, Centre for Nanostructures and Advanced Materials, DSI-CSIR Nanotechnology Innovation Centre, Council for Scientific and Industrial Research (CSIR), Pretoria, South Africa
[3] Chemical Cluster, Pharmaceutical Biotechnologies, Council for Scientific and Industrial Research (CSIR), Pretoria, South Africa
[4] Department of Microbiology, Virology Laboratory, Faculty of Natural and Agricultural Sciences, North-West University, Mafikeng, South Africa
[5] Department of Human Physiology, Nelson Mandela University, Port Elizabeth, South Africa
[6] Material Science, Innovation and Modelling (MaSIM), Faculty of Natural and Agricultural Sciences, North-West University, Mmabatho 2735, South Africa
[*] Author to whom any correspondence should be addressed.

E-mail: successfreak01@gmail.com

Keywords: antiviral activity, cytotoxicity, herpes simplex virus type 2, nanomedicine, nanoparticles

Supplementary material for this article is available online

Abstract

Herpes simplex virus type 2 (HSV-2) remains a significant public health concern due to its high rates of mortality and morbidity. While various chemotherapeutic options exist for treating HSV-2, they are often inadequate as none provide a definitive cure, and there is a growing issue of drug-resistant strains. The introduction of nanomedicine for antiviral drug delivery offers a promising avenue to enhance the effectiveness of these treatments. This study explored an innovative approach to treating HSV-2 by encapsulating valacyclovir in biodegradable polycaprolactone (PCL) using a double emulsion technique. The formulated valacyclovir-loaded polymeric nanoparticles were characterized, revealing monodispersed particles with an average hydrodynamic size ranging from 154.9 $\pm$ 2.1 to 232.8 $\pm$ 6.2 nm, along with an encapsulation efficiency of 50%–66% and a drug loading capacity of 11.6%–13.9%. Additionally, there is no significant cytotoxicity of the test compounds to Vero cells at 0.3 mg ml^{-1} concentration with a cell viability within the range of 85 $\pm$ 13.6%−100 $\pm$ 4.8%. The antiviral activity of both the free drug (valacyclovir) and the valacyclovir-loaded polymeric nanoparticles was assessed in HSV-2 infected Vero cells. The results demonstrated that the valacyclovir-loaded nanoparticles exhibited a 1.2–1.3fold ($p < 0.005$) increase in antiviral efficacy compared to the free drug. This study thus presents a novel nanotechnology-based treatment approach for HSV-2, offering enhanced antiviral effectiveness over traditional treatments.

1. Introduction

A recent report by the World Health Organization has emphasized the urgent need to develop new strategies, such as, vaccines, microbicides, and antiviral agents for both the prevention and treatment of herpes simplex virus type 2 (HSV-2) infections [1]. This call to action stems from the rising global prevalence of HSV-2, which affects approximately 13% of individuals under the age of 50, as well as the associated risks of comorbidities and the increased likelihood of acquiring or transmitting HIV [1]. HSV-2 primarily affects the anogenital region and establishes latency in the neural ganglia [2]. The virus's genetic adaptability has allowed it to develop resistance to antiviral agents, leading to the emergence of

new HSV-2-resistant strains [3]. Although nucleoside analogues have been somewhat useful in treating HSV-2, there has been a concerning rise in drug-resistant strains [4, 5]. For instance, prolonged acyclovir treatment in immunocompromised patients has been linked to mutations in the viral thymidine kinase or DNA polymerase genes, resulting in acyclovir resistance [5]. Several attempts have been carried out to revolutionize the treatment of HSV using monoclonal antibody (mAbs), however, no mAbs have been approved by the US Food and Drug Administration (FDA) for the treatment of HSV associated infections. In a study conducted by Seyfizadeh and colleagues, where they carried out a phase 2 clinical trial on HDIT10, a humanized IgG targeting HSV-1/2 gB with the aim of comparing the safety and efficacy of a single dose infusion of HDIT10 to valacyclovir (VCV) treatment in patients with the history of HSV-2 infection. HDIT10 did not show significant efficacy over valacyclovir which is the standard of care treatment for HSV-2 [6].

Valacyclovir hydrochloride (valacyclovir), an L-valyl ester of acyclovir, was approved by the FDA in 1995 for the treatment of herpes simplex virus and herpes zoster infections. While its antiviral potency is comparable to that of acyclovir, valacyclovir hydrochloride offers improved pharmacokinetic properties [7]. Upon administration, valacyclovir hydrochloride is converted to acyclovir and L-valine by esterase during first-pass metabolism [8]. However, its stability decreases in more basic environments, which negatively impacts the its bioavailability by breaking down the drug into active acyclovir and L-valine [7]. Valacyclovir also improves oral bioavailability, achieves higher plasma levels, and reduces dosing frequency by increasing acyclovir's lipophilicity [9, 10]. Although well-tolerated, valacyclovir requires a high dose to be effective against HSV-2, with few adverse effects reported [11]. Therefore, it is crucial to explore new methods to enhance the antiviral efficacy of valacyclovir hydrochloride.

Nanotechnology offers promising solution for modifying the development of new materials into their nanoforms, with various applications in the fields of biosensing and drug delivery [12, 13]. Nanoparticles in particular, can address the limitations of conventional pharmaceutics by reducing drug toxicity, improving bioavailability and enhancing the uptake of insoluble drugs [4, 14, 15]. The unique surface area to volume ratio and the surface charge of nanoparticles facilitates interactions with cell membranes, making them a valuable tool in antiviral treatments [4, 16, 17]. Moreover, drug loaded nanoparticles are faced with some challenges like the non-specific phagocytic uptake of some of the nanoparticles which may hinder the therapeutic effect of the administered drug. Also, studies have shown that drug delivery via sustained release may be possible for a short period and the leakage of encapsulated drug may also reduce the antiviral activity of the drug [17, 18]. Despite these challenges, several studies have highlighted the potential of nanoparticles as a preventive strategy against HSV infection [19, 20]. Given the antiviral potential of valacyclovir and the advantages of nanoparticles, this study focused on designing polymeric nanoparticles containing valacyclovir hydrochloride and evaluating their antiviral activity against wild-type HSV-2.

2. Materials and methods

2.1. Materials

Valacyclovir hydrochloride (VCV ⩾98% HPLC) was purchased from DB Fine Chemicals (Sandton, South Africa), polycaprolactone (PCL) 14000 Mw, polycaprolactone diol (Mw 2000), N, N'-diisopropylcarbodiimide (DIC), 4-(dimethylamino)-pyridin (DMAP), N-hydroxysuccinimide (NHS)/hydroxybenzotriazole (HOBT), N, N-dimethylformamide (DMF), ethyl acetate (EA, high performance liquid chromatography (HPLC) grade), span 80, polyvinyl alcohol (PVA), rhodamine B (rhod-B), and penicillin-streptomycin (10 000 U ml^{-1}) were purchased from Sigma-Aldrich (Johannesburg, South Africa). MTT reagent (3-(4,5-dimethylthiazol-2-yl)-2,5-diphenyl tetrazolium bromide) was purchased from Promega (Anatech, South Africa). Phosphate buffered saline (PBS), Dulbecco's modified Eagle medium (DMEM), and fetal bovine serum (FBS) were purchased from Thermo fisher Scientific (Johannesburg, South Africa). All reagents used were of analytical and HPLC grade.

2.2. Cells and virus strain

Vero cells (African Green Monkey) purchased from ATCC were used for the propagation of wild-type HSV-2 strain as well as titration and neutralization of the virus. HeLa and SiHa cell lines (cervical carcinoma cell lines) were used for the *in vitro* cell uptake study. The cells were maintained in DMEM supplemented with 10% FBS and 0.5% antibiotics (penicillin-streptomycin). The wild-type HSV-2 strain was obtained from the Next-Generation Health cluster laboratory at the Council for Scientific and Industrial Research (CSIR, Pretoria, South Africa). The virus titer was evaluated by an end-point dilution assay as previously described [21], and stored at −80 °C until ready for use.

2.3. Preparation of PCL-rhod-B conjugates

The conjugation of rhod-B to PCL diol (rhod-B-PCL) was conducted by condensation reaction as described in a previous study [22]. Briefly, PCL diol (500 mg, 1.0 equiv.), Rhodamine B (144 mg, 1.2 equiv.), DIC (113 mg, 3.0 equiv.), NHS/HOBT (113 mg, 3 equiv.) and DMAP were dissolved in 10 ml

of N, N-dimethylformamide (DMF) under continuous stirring in the dark for 48 h at room temperature. The mixture was transferred to a rotary evaporator to remove the organic solvent. The unreacted rhodamine B was removed by washing the product with a mixture of ethanol and PBS (1:2) and air-dried under low heat.

2.4. Preparation of nanoparticles

Valacyclovir-loaded polymeric nanoparticles (PCL-VCV-NPs) and drug-free NPs (PCL-NPs) were prepared using the double emulsion solvent evaporation technique [23]. PCL-VCV-NPs were prepared at different drug-to-polymer ratio, with more focus on NF1 (1:1), NF2 (1.5:1), and NF3 (2:1). Briefly, 10 mg of PCL dissolved in an organic solvent (ethyl acetate, EA) containing span 80 and 10 mg of VCV dissolved in distilled water were mixed under continuous stirring at 250 rpm for 5 min. The solution was transferred into a 250 ml beaker containing 10 ml PVA and homogenized at 12 500 rpm with a high-speed homogenizer (Labfeng, FSH-2 A, China). The emulsion was stirred overnight to remove the organic solvent and then freeze-dried to form lyophilized nanoparticles. The same method was used to prepare valacyclovir-loaded polymer-rhodamine nanoparticles (VCV-PCL-rhod-B-NPs). That is, 1% of PCL-rhod-B conjugates described above (section 2.3) was added to PCL to prepare the nanoparticles.

2.5. Characterization of nanoparticles

A Malvern Zetasizer Nano ZS (Malvern Instruments, Worcestershire, UK) was used to measure the hydrodynamic diameter (particle size), nanoparticle distribution polydispersity index (PDI) and the surface charge zeta potential (ZP) of PCL-VCV-NPs. The NPs were dissolved in distilled water, placed in a disposable cuvette and measured at ambient temperature at a backscattered angle of 173° using Mark–Houwink parameters. A triplicate measurement of all the nanoparticles was conducted and the data was represented as the mean and standard deviation (SD). The morphology of the nanoparticles was determined using a scanning electron microscope (field emission scanning electron microscope (FESEM) (JEOL JSM-7500, Japan)) by attaching the nanoparticles to the carbon stubs and a conductive carbon coating applied to the nanoparticles through a high vacuum evaporator under atmospheric argon. A Fourier transform infrared (FTIR) spectroscopy (Perkin Elmer, Waltham, MA, USA) was used to determine the functional groups of the samples (VCV, PCL, PCL-NPs and PCL-VCV-NPs) by placing them onto the FTIR plate, and the spectra against an air spectrum background were recorded at a wavenumber of 4000–400 cm^{-1}. The thermal properties of the samples were determined with differential scanning calorimetry (DSC) (Q2000, TA Instruments, Haverhill, MA, USA) and thermogravimetric analyzer (TGA) (5500, TA Instruments, New Castle, USA) at a temperature scan rate of 10 °C min^{-1}. The powder x-ray diffraction (PXRD) of the samples was determined using a PANalytical X'Pert PRO diffractometer (Phillips, Lelyweg, Netherlands). The x-ray source, Cu Kα ($\lambda = 1.5406$ Å) was operated at 40 kV and 40 mA at a scanning rate of 2° min^{-1} [24]. The crystallite size was calculated using the Scherrer equation and the XRD density of the prepared PCL-VCV-NPs were examined using x-ray diffraction peaks. ^{1}H nuclear magnetic resonance (NMR) spectra of PCL-rhod-B conjugate were obtained from a Varian 600 MHz spectrometer (Varian Inc. California, USA) with Varian NMR spectra console operated by the host software (Unity INOVA/Solaris 7) and equipped with a 5 mm HX probe at room temperature using chloroform ($CDCl_3$) as the dissolution solvent. The chemical shifts of the conjugates were recorded as parts per million (ppm).

2.6. Evaluation of encapsulation efficiency and drug loading capacity

HPLC (Shimadzu, USA) was used for the estimation of the drug loading capacity and encapsulation efficiency of PCL-VCV-NPs. The solution of the nanoparticles was prepared in PBS, spun with a benchtop centrifuge at 10 000 rpm for 15 min and the amount of drug in the supernatant was determined. An isocratic chromatographic system was set up according to a previously established protocol with some modifications [9]. Briefly, the HPLC was calibrated with a standard solution of VCV at a concentration ranging from 40 to 160 μg ml^{-1} and the amount of drug in the solution was determined. A mobile phase of 70:30 v/v methanol and distilled water containing trimethylamine (pH 7) was prepared at a flow rate of 0.15 ml min^{-1} with injection volume of 10 μl and a wavelength of 257 nm,

$$\text{Encapsulation efficiency}(\%) = \frac{\text{Amount of drug in solution}}{\text{Total amount of drug}} * 100$$

$$\text{Drug loading} = \frac{\text{Mass of drug}}{\text{Total mass of drug} - \text{loaded NPs}} * 100.$$

2.7. *In vitro* drug release study

The release profile of the drug entrapped in PCL and the free drug in solution was determined using the HPLC protocol described above (section 2.6). A 1 mg ml^{-1} concentration of PCL-VCV-NPs was prepared by dissolving 10 mg of the nanoparticles in 10 ml of PBS at pH 7.4 and placed in a shaking waterbath at 37 °C at 120 rpm. A 2 ml aliquot was taken at predetermined time intervals between 0 and 24 h and replaced with the same volume of PBS after each withdrawal. The collected aliquots were filtered and analyzed on the HPLC instrument.

2.8. Cytotoxicity assay

To determine the toxicity of VCV (pure drug), PCL-NPs and PCL-VCV-NPs, a viability test using the MTT assay kit on Vero cells was conducted according to a previously established protocol [25]. Briefly, 10 000 Vero cells were seeded in a 96 well plate for 24h, after which, the cells were treated with three-fold serial dilutions of VCV, PCL-NPs and PCL-VCV-NPs at a starting concentration of 1 mg ml^{-1} and incubated for 72 h. Thereafter, 25 µl MTT reagent (0.5 mg ml^{-1}) was added to the cells and incubated for 3 h at 37 °C, 5% CO_2. The media was then replaced with 100 µl DMSO to dissolve formazan crystals and the absorbance was measured spectrophotometrically at dual wavelengths (450/620 nm) using a Tecan Infinite F500 plate reader. The cell viability was determined using the formula:

$$\text{cell viability } (\%) = \frac{\text{Absorbance of treated cells} - \text{Absorbance of the background}}{\text{Absorbance of untreated cells} - \text{Absorbance of the background}} * 100.$$

2.9. Virus neutralization assay

The inhibition of HSV-2 was determined using Vero cells following a previously described protocol with some modifications [26]. Briefly, 10 000 cells/well were seeded in growth media in triplicates in 96-well plates and incubated at 37 °C, 5% CO_2 for 24 h. The media was removed and the cells were washed three times with PBS. Then 50 µl of the $TCID_{50}$ of wild-type HSV-2 was added to the cells and incubated for 1 h. Then a three-fold dilution of the test compounds (VCV, PCL-NPs and PCL-VCV-NPs) prepared in DMEM containing 2% FBS, 1% penicillin-streptomycin, was added and incubated at 37 °C, 5% CO_2 for 72 h. Thereafter, cells were washed twice with PBS and 25 µl of MTT solution (0.5 mg ml^{-1}) was added to each wells and incubated for 3 h at 37 °C, 5% CO_2. The solution was then replaced with 100 µl DMSO and the plate was measured spectrophotometrically at dual wavelengths (450/620 nm) using a Tecan Infinite F500 plate reader.

2.10. Statistical analysis

All statistical analyses were carried out using GraphPad Prism Software 5.0 (GraphPad San Diego, CA, USA). The half-maximal inhibitory concentration (IC_{50}) of PCL-VCV-NPs and VCV-PCL-rhod-B was calculated using log-logistic regression analysis. One-way analysis of variance (ANOVA) followed by a Bonferroni post hoc test was also used to compare the statistical significance between the inhibitory concentrations of the treated and untreated cells. *p*-values of $\leqslant 0.05$ were considered statistically significant.

3. Results and discussion

3.1. Characterization of nanoparticles

3.1.1. Hydrodynamic size, PDI and ZP

PCL-VCV-NPs were synthesized using the double emulsion solvent evaporation technique. The nanoparticle size, PDI and ZP of PCL-VCV-NPs (NF1, NF2, and NF3), PCL-NPs, and VCV-PCL-rhod-B were characterized using Malvern Zetasizer Nano ZS and the values obtained are illustrated in table 1 and figure S3. All samples showed compact nanoparticle sizes ranging from of 154.9 ± 2.1–232.8 ± 6.2 nm. The hydrodynamic size of PCL-VCV-NPs increased proportionally with the drug concentration. This finding aligns with the study by Huang and colleagues [27], which also reported that drug concentration significantly influences the size of nanoparticles.

The increase in the particle size of PCL-VCV-NPs compared to the drug free polymer nanoparticles (PCL-NPs), further indicates successful drug entrapment within the polymer matrix. The nanoparticles, reflected by the PDI, is a key a factor in determining the uniformity and monodispersity of the encapsulated drug as well as the consistency of nanoparticle size within the nanosystem. All samples demonstrated uniform and monodisperse distribution with PDI values of less than 0.3. This uniformity is essential for effective drug delivery, as a wide range of particle sizes, or polydispersity, could negatively affect the therapeutic efficiency of the nanoparticles. Larger nanoparticles in a polydisperse system may be phagocytosed by macrophages, while smaller ones might be internalized by cells through passive uptake [28, 29].

Furthermore, the average ZPs (surface charge) of all the samples ranged from −8.1 ± 0.3 to −16.3 ± 0.8. The negative charge observed across all samples is likely due to the presence of terminal carboxylic groups present in the PCL. While a positive ZP value would enhance nanoparticle penetration into cell membranes, potentially disrupting membrane integrity and increasing cell toxicity, negatively charged nanoparticles are less likely to penetrate cellular membranes, thereby reducing their potential to damage cells [30, 31]. It is noteworthy that drug-loaded nanoparticles can become unstable through molecule/protein adsorption when dispersed in a complex biological system, resulting in the formation of aggregates [32]. However, the dissolution of PCL-VCV-NPs in the cell culture media did not show any agglomeration during cell treatments for 48 h.

Table 1. Average particle size, PDI and zeta potential of formulated nanoparticles and conjugates.

Nanoparticle code	Loaded drug	Polymer	Drug/polymer ratio	Particle size (nm)	PDI	ZP (mV)	EE (%)	DLC (%)
NF1	VCV	PCL	10 mg: 10 mg (1:1)	205.7 ± 3.5	0.255 ± 0.01	−14.0 ± 0.3	66	11.6
NF2	VCV	PCL	15 mg: 10 mg (1.5:1)	213.2 ± 6.5	0.245 ± 0.02	−16.3 ± 0.8	50	12.5
NF3	VCV	PCL	20 mg: 10 mg (2:1)	232.8 ± 6.2	0.200 ± 0.02	−12.5 ± 3.4	51	13.9
PCL-NPs	N/A	PCL	N/A	210.3 ± 2.0	0.162 ± 0.01	−8.1 ± 0.3	N/A	N/A
PCL-VCV-rhod-B	VCV	PCL-rhod-B	10 mg: 10 mg (1:1)	154.9 ± 2.1	0.09 ± 0.01	−9.6 ± 1.0	N/A	N/A

EE: encapsulation efficiency, DLC: drug loading capacity, N/A: not applicable.

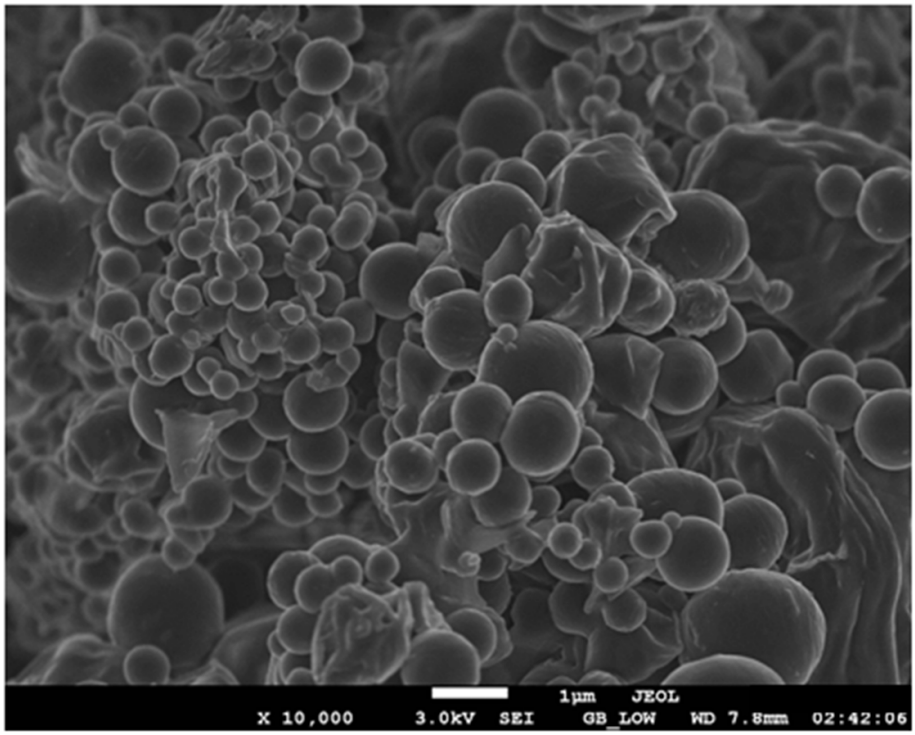

Figure 1. Field emission scanning electron microscopy of PCL-VCV-NPs. The photomicrograph showed clumps or nanoparticle aggregates with varied sizes.

Additionally, more than half of the drug was successfully loaded into the polymer, as indicated by the encapsulation efficiency (50%–66%) and drug loading capacity (11.6%–13.9%) across all formulated nanoparticles (PCL-VCV-NPs).

3.1.2. Morphology

The morphological characteristics of the optimized PCL-VCV-NPs were analyzed using FESEM. The shape of nanoparticles is known to significantly affect their interaction with cells and their the flow properties [33]. As shown in figure 1, PCL-VCV-NPs exhibited a spherical shape with both smooth and rough edges. The average size of PCL-VCV-NPs calculated through FESEM (217.4 ± 20.4 nm) does not differ significantly from the hydrodynamic size obtained using dynamic light scattering (DLS).The presence of nanoparticle aggregates in the SEM image suggests potential nanoparticle agglomeration, which is consistent with the small ZP values observed. These ZP values, reported from the DLS analysis in table 1, indicate that lower ZP can lead to increased nanoparticle aggregation. Furthermore, NP agglomeration may affect the interaction between cells and nanoparticles, reducing the activity of the encapsulating drug. The aggregation seen in the SEM images is likely due to the sample preparation process. Specifically, the nanoparticles underwent freeze-drying and were directly mounted onto carbon stubs using double-sided adhesive carbon tape. Such preparation methods can induce particle aggregation due to the removal of the aqueous medium and the forces exerted during drying and mounting. Therefore, the aggregation observed in the SEM images does not reflect the behavior of the nanoparticles under physiological conditions. To address this potential issue, modifying parameters such as surface charge, hydrophobicity, that is, the use of low molecular weight polymers (PCL), stabilizing agents and spray-drying of NPs can limit nanoparticle

agglomeration and produce nanostructures that are less prone to aggregation.

3.1.3. FTIR analysis

The FTIR spectra results of VCV, PCL, PCL-NPs and PCL-VCV-NPs are presented in figure 2, where the functional groups of each component were analyzed. The similar peak intensities observed between PCL and PCL-NPs indicate successful nanoparticle formulation. However, when VCV was incorporated into PCL-NPs, shifts in peak intensities were observed at both lower and higher wavenumbers. For example, shifts were noted in the vibrational asymmetric and symmetric C–H stretching of PCL-VCV-NPs at 2911.5 cm^{-1} and 2856.7 cm^{-1}, along with the presence of broad O–H stretching at 3323.6 cm^{-1}. Additionally, new peaks appeared at 1634 cm^{-1} and 1485.9 cm^{-1}, corresponding to C=C stretching and C–H bending respectively, in positions similar to those of VCV, indicating successful entrapment of VCV within the polymer. Moreover, some prominent peak intensities present in VCV were absent in the FTIR spectra of PCL-VCV-NPs. This disappearance is likely due to the encapsulation of VCV within the polymer matrix, which may have masked the presence of these functional groups during analysis.

3.1.4. Thermal analyses

The thermal properties of PCL, PCL-NPs, and PCL-VCV-NPs were analyzed and compared to the pure drug (VCV) to understand how the nanoparticles respond to changes in heat flow and temperature. Two thermal analysis techniques were employed; DSC and TGA. DSC was used to determine the structural conformational changes in PCL, PCL-NPs, VCV and PCL-VCV-NPs, as the transition stages in nanomaterials are often influenced by their material composition [34]. In figure 3(A), the DSC thermogram of VCV displayed two prominent endothermic peaks at 92.7 °C and 131.4 °C, and one exothermic peak at 211.5 °C. The broad endothermic peak at 92.7 °C likely represents the transition stage of VCV, which may be due to the dehydration of crystal water within the VCV structure. The distinct endothermic peak suggests that this water is binding water rather than surface absorbed water [35]. The endothermic peak at 131.4 °C corresponds to the melting point of VCV before recrystallization, while the sharp exothermic peak indicates the thermal decomposition of residual VCV after crystal melting. Figure 3(B) illustrates the first heating process of PCL, PCL-NPs, and PCL-VCV-NPs, revealing a sharp endothermic peak corresponding to the melting and decomposition temperature of PCL at 64.4 °C. PCL-NPs displayed a melting peak at 54.1 °C, while PCL-VCV-NPs showed two endothermic peaks at 52.9 °C and 183.8 °C. These two peaks in PCL-VCV-NPs suggest a eutectic behavior, resulting from the mixture of VCV with PCL.

Figure 3(C) depicts the cooling stage following the first heating process of PCL, PCL-NPs, and PCL-VCV-NPs. Both PCL and PCL-NPs exhibited crystallization peaks similar to the melting peak area of PCL, although the crystallization peak of PCL-NPs was reduced. In contrast, the cooling process of PCL-VCV-NPs did not show any crystallization peak, instead displaying an amorphous solidification of the nanoparticles. This indicates the crystalline nature of PCL and PCL-NPs, while PCL-VCV-NPs exhibit an amorphous structure. During the second heating process, following the cooling stage (figure 3(D)), all samples showed a single endothermic peak at 52.9 °C. Notably, the melting peak of PCL shifted from 64.4 °C in the first heating to 52.9 °C in the second heating. The endothermic peak observed in the first heating of PCL-VCV-NPs at 183.8 °C was not retained during the second heating, with only the melting peak similar to that of PCL remaining. This suggests that VCV is well-dispersed within the polymer and is compatible with PCL.

TGA was used to monitor the changes in PCL, PCL-NPs, VCV and PCL-VCV-NPs that is due to mass loss and water content when the samples were heated at a controlled rate of 10 °C min^{-1}. Figure 4 illustrates the TGA curves of PCL, PCL-NPs VCV and PCL-VCV-NPs. The TGA curve of PCL showed no significant weight loss below 100 °C, indicating that the polymer did not absorb surface moisture. Moisture absorption in polymers can lead to water molecules interacting with the polymer, potentially causing cleavage of chemical bonds and accelerating polymer degradation [36]. In contrast, the TGA curves for VCV, PCL-NPs, and PCL-VCV-NPs exhibited weight losses of approximately 8.5%, 1.5%, and 4.7% respectively, within the temperature range of 30 °C–120 °C. These weight losses are attributed to the dehydration of water molecules or moisture content present in the samples. Furthermore, the TGA curve of VCV showed three distinct weight loss stages, while PCL-NPs and PCL-VCV-NPs exhibited two stages, and PCL had just one stage. These findings correspond with the DSC results previously described.

3.1.5. PXRD analysis

The structural characteristics of all samples, including PCL, PCL-NPs, VCV and PCL-VCV-NPs were determined using PXRD. PXRD evaluates the crystalline and amorphous nature of the samples by measuring the geometric scattering of radiation from the crystal planes. As shown in figure 5, the PXRD pattern of PCL displays two sharp peaks at 21.7° and 24° assigned to the (100) and (200) orthorhombic crystallographic planes, respectively. These peaks were also observed in the PCL nanoparticles (PCL-NPs), albeit with reduced intensities. The diffractogram of VCV

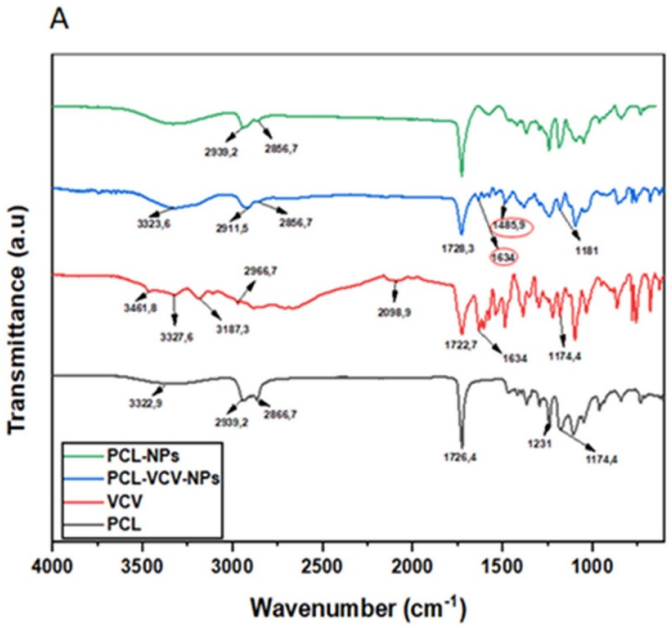

B

Functional group description	PCL	VCV	PCL-VCV-NPs	PCL-NPs
	IR Absorption frequency (cm^{-1})			
Asymmetric C-H stretching	2939.2	–	2911.5	2939.2
Symmetric C-H stretching	2866.7	–	2856.7	2856.7
C=O stretching	1726.4		–	
N-H stretching	3322.9	3461.8; 3327.6	–	
C-H stretching	–	3187.3; 2966.7	–	
C-O-C stretching	1231; 1174.4	1174.4	1171.4	
O-H stretching			3323.6	
C—H bending		1485.9	1485.9	
C=C stretching		1634	1634	

Figure 2. FTIR spectra of (A) PCL, VCV, PCL-NPs and PCL-VCV-NPs. (B) The variation of characteristic infrared (IR) peaks of PCL, VCV, PCL-NPs and PCL-VCV-NPs obtained from FTIR spectroscopy at a wavenumber range of 4000–400 cm^{-1}.

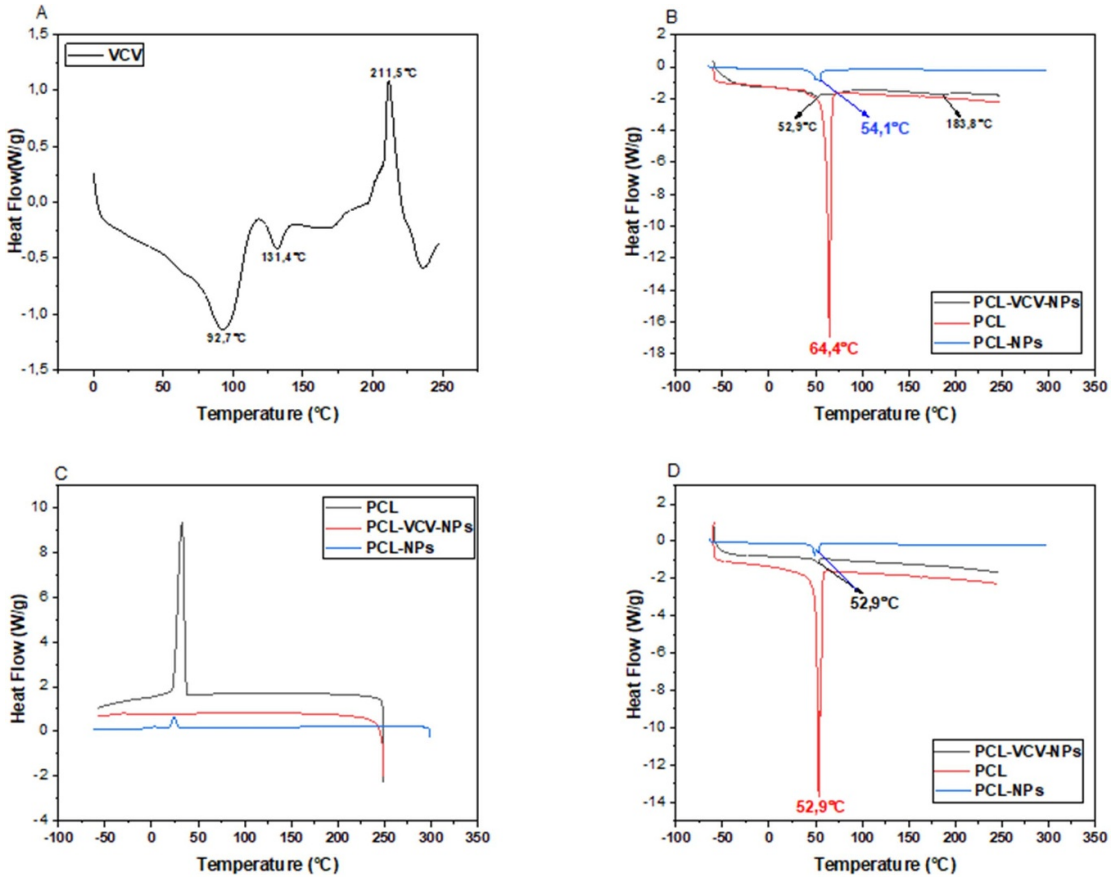

Figure 3. DSC thermograms of (A) VCV, (B) first heating of PCL, PCL-NPs and drug-loaded polymeric nanoparticles (PCL-VCV-NPs), (C) crystallization behavior of PCL, PCL-NPs and PCL-VCV-NPs after cooling of the first heating (melt) to −60 °C, and (D) second heating of PCL and PCL-VCV-NPs. The cooling, first and second heating were conducted at 10 °C min^{-1}.

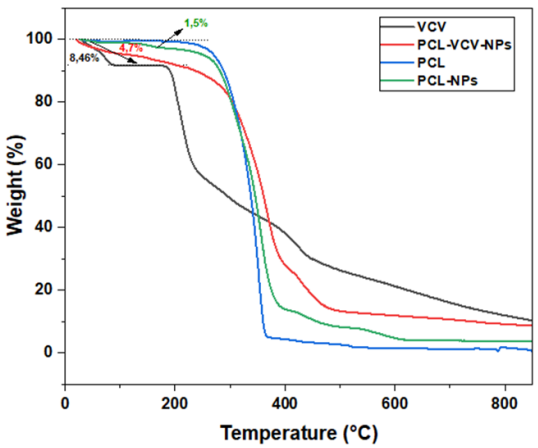

Figure 4. Thermogravimetric analysis (TGA) curve of PCL, PCL-NPs, VCV and PCL-VCV-NPs at a controlled heating rate of 10 °C min^{-1}.

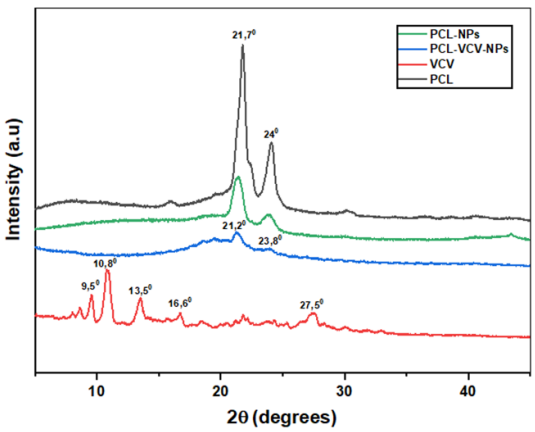

Figure 5. PXRD diffractogram of VCV, PCL, PCL-NPs and lyophilized valacyclovir-loaded polymeric nanoparticles (PCL-VCV-NPs).

exhibited multiple sharp peaks that aligns with the 2θ characteristic peaks of the sesquihydrate (SH) crystal form of valacyclovir hydrochloride, as reported by Wu and colleagues [35]. However, these diffraction peaks of VCV were absent in the PXRD pattern of PCL-VCV-NPs. The disappearance of VCV's characteristic peaks, along with the reduced peak intensities and shifts at 21.2° and 23.8° (similar to those of PCL), further confirm the reduced crystalline nature of PCL-VCV-NPs. The reduced crystallinity and the crystallite size of PCL-VCV-NPs (7.15 ± 8.5 nm) are considered as the direct reason

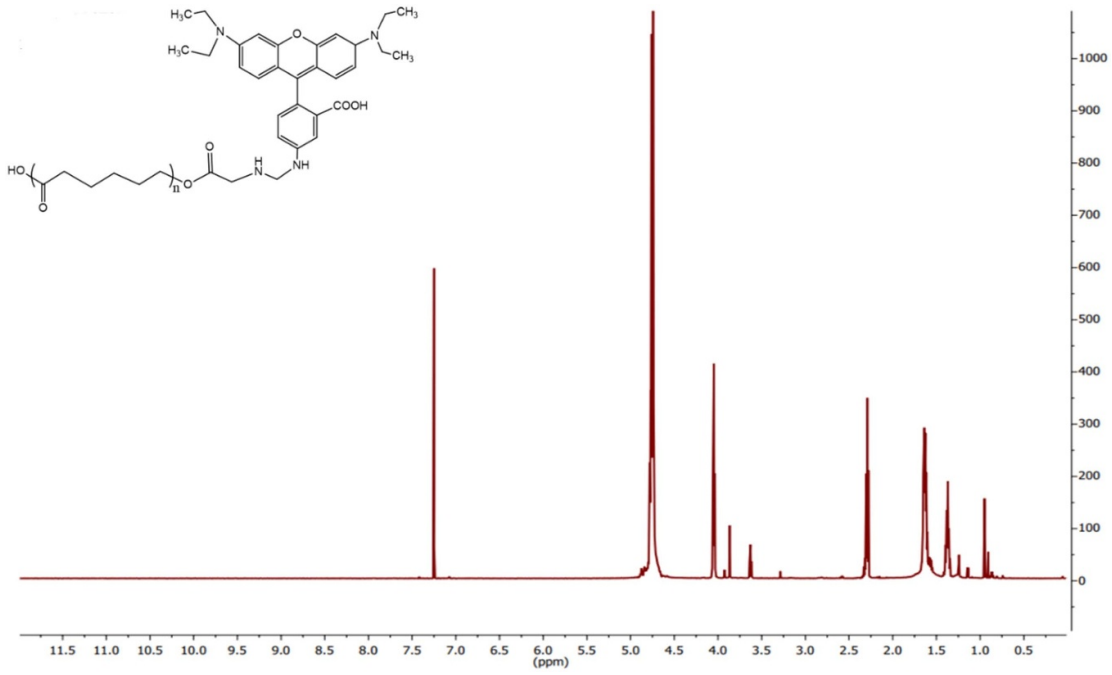

Figure 6. ^{1}H NMR spectra of synthesized PCL-rhod-B conjugate in chloroform-d ($CDCl_3$).

Table 2. Estimation of the crystallite size of PCL-VCV-NPs from PXRD diffractogram.

Formulation	Peak position 2θ (°)	Peak position θ (°)	FWHM β (°)	Crystallite size (nm)	Average crystallite size (nm) of PCL-VCV-NPs
PCL-VCV-NPs	21.2	10.6	064 054	1317 700 335	7.15 ± 8.5
	23.8	11.9	750 511	1126 468 215	

for the reduced peak intensities. The estimated x-ray density of PCL-VCV-NPs diffraction peaks is zero (table S2), suggesting that PCL-VCV-NPs is tending towards the amorphous region. The PXRD results corroborate the findings from the DSC analysis, suggesting the dispersion of the drug within the polymer.

3.1.6. ^{1}H-NMR spectra analysis of PCL-rhod-B conjugate

The proton NMR spectrum of PCL-rhod-B was used to confirm the successful conjugation of rhodamine-B to PCL diol. The characteristic NMR peaks of PCL-rhod-B recorded using Varian 600 MHz spectrometer are shown in figure 6, and the allocation of each NMR spectrum is represented in table 2. The signal peaks of rhodamine B and PCL-diol in the NMR spectra of PCL-rhod-B conjugates are consistent with the peak values that were previously reported in the literature [37, 38]. Four distinct peaks/signals of PCL-diol corresponding to the four proton environments within the polymer chain are observed. The carbonyl-adjacent methylene protons (H7) resonate at a chemical shift of 4.06 ppm due to the electron-withdrawing effect of the carbonyl group. The methylene protons alpha to the carbonyl group (H8) appear at a slightly lower chemical shift at 2.30 ppm. The methylene protons within the polymer chain (H9 and H10) resonate at the lowest chemical shifts of 1.63 and 1.36 ppm, respectively. The relative intensities of the peaks in the proton NMR spectrum reflect the relative abundance of each proton environment within the polymer chain. Of the signals of PCL-diol, the H9 and H10 protons are the most abundant, followed by the H8 protons, while the H7 protons are the least abundant. Similarly, the multiple peaks of rhodamine B that are assigned to different proton environments showed some aromatic protons on the xanthene ring that resonate at the highest chemical shifts (table 3), followed by the methyl and methylene protons on the dimethylamine groups. The ethyl protons resonate at the lowest chemical shifts. All these observed signals confirmed the successful conjugation of rhodamine B to PCL-diol.

3.2. *In vitro* release of PCL-VCV-NPs

The *in vitro* release of VCV from PCL-VCV-NPs was evaluated in phosphate buffered saline (pH 7.4) over a 24 h period. As depicted in figure 7, the release profile of VCV exhibited an initial rapid release from the polymer, followed by more controlled release. Within

Table 3. Allocation of chemical shifts to PCL-rhod-B conjugate.

Proton	Chemical shift (δ ppm)	Assignment
H1	7.40	Aromatic proton on xanthene ring
H2	7.25	Aromatic proton on xanthene ring
H3	6.95	Aromatic proton on xanthene ring
H4	3.62	Methyl group on dimethylamine
H5	1.24	Ethyl group on dimethylamine
H6	1.17	Ethyl group on dimethylamine
H7	4.06	Methylene proton adjacent to the carbonyl group (–CH_2OCO–)
H8	2.30	Methylene proton alpha to the carbonyl group (–$OCCH_2$–)
H9	1.63	Methylene proton within the polymer chain (–CH_2CH_2–)
H10	1.36	Methylene proton within the polymer chain (–CH_2CH_2–)

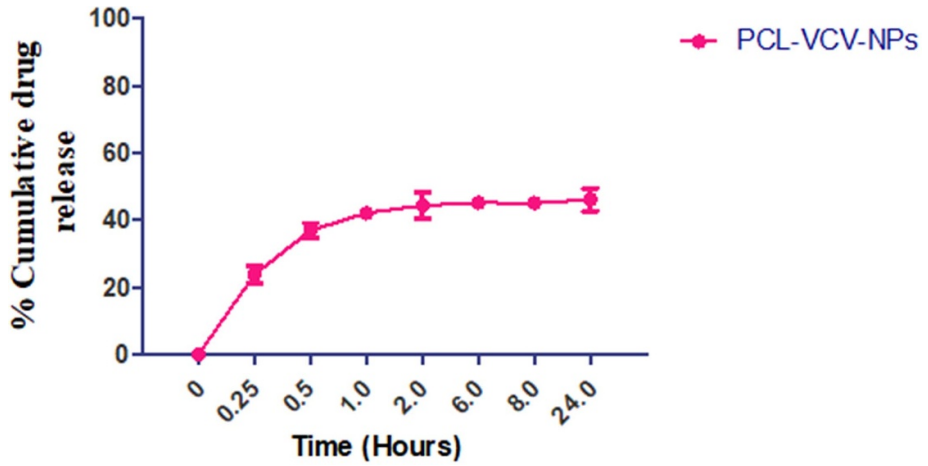

Figure 7. *In vitro* release of valacyclovir hydrochloride (VCV) from PCL-VCV-NPs in phosphate buffered saline (pH 7.4) under continuous agitation at 120 rpm, 37 °C for 24 h. Data represents the mean ± standard deviation of the experiments.

the first 30 min (0.5 h) of the experiment, approximately 40 ± 3.7% of the drug was released into the dissolution medium. The burst release of VCV may be a result of the drug's adsorption onto the surface of the polymer. Drug molecules attached to the surface of nanoparticles are more easily released into the dissolution medium than those entrapped within the polymer [39, 40]. In addition, the small crystallite size of PCL-VCV-NPs (table 2) also supports the release rate of VCV, as small crystallite size dissolves faster, which may also be associated with a faster release rate. After 24 h of constant agitation and incubation at 37 °C, approximately 50 ± 5.8% of VCV was released from PCL-VCV-NPs. One probable reason for the decrease in the release rate of the drug may be due to the rigidity and the molecular weight of the polymer. PCL is a rigid polyester, requiring more time for hydrolysis to take place, which may further influence the drug release rate. In addition, the use of non-ionic surfactant (span 80) during the preparation of PCL-VCV-NPs may act as a storehouse for the entrapped drug, reducing the outflow of the drug from the nanoparticles into the dissolution medium. This may not necessarily be the case in this study as the concentration of surfactant used was insignificant, however, Surya Teja and colleagues emphasized that an increase in the concentration of surfactant decreases the drug release rate [41]. The chromatogram of the detection of VCV at a wavelength of 257 nm, the retention time of 9.5 min and the regression analysis table are shown in the supplementary list (table S1, figures S1 and 2). To better understand the release phenomena of PCL-VCV-NPs, multiple kinetic drug release models were utilized to assess the release of VCV from PCL-VCV-NPs (table 4). Zero order, first order, Weibull, Higuchi, Gompertz, Hopfenberg, Hixson–Crowell, and Korsmeyer–Peppas release profiles were used in Microsoft Excel® to confirm the right release kinetics for the PCL-VCV-NPs, followed by regression analysis. The release kinetics of PCL-VCV-NPs formulations were best represented by the Weibull model ($R^2 \geqslant 0.98$), indicating a swelling-controlled release of the encapsulated drug. In this situation, the encapsulated drug (VCV) diffuses from the polymer matrix to the surrounding medium via PCL swelling and degradation. To improve the drug delivery system, the authors would like to suggest the addition of porogens to the matrix of the polymer which creates polymeric pores within the matrix influencing drug diffusion and release. In addition, the modification of the polymer properties with the use of blends and co-polymers (PEG) can adjust the rheological behavior of PCL by enhancing the segmental mobility of the PCL chains to influence drug release from the

Table 4. R^2 value of the drug release of valacyclovir hydrochloride from PCL-VCV-NPs.

Formulation	Zero order	First order	Higuchi's model	Korsmeyer–Peppas model	Weibull model	Hopfenberg model	Gompertz model	Hixson–Crowell model
PCL-VCV-NPS	0.4989	0.6020	0.6440	0.7892	0.9856	0.6014	0.8230	0.5571

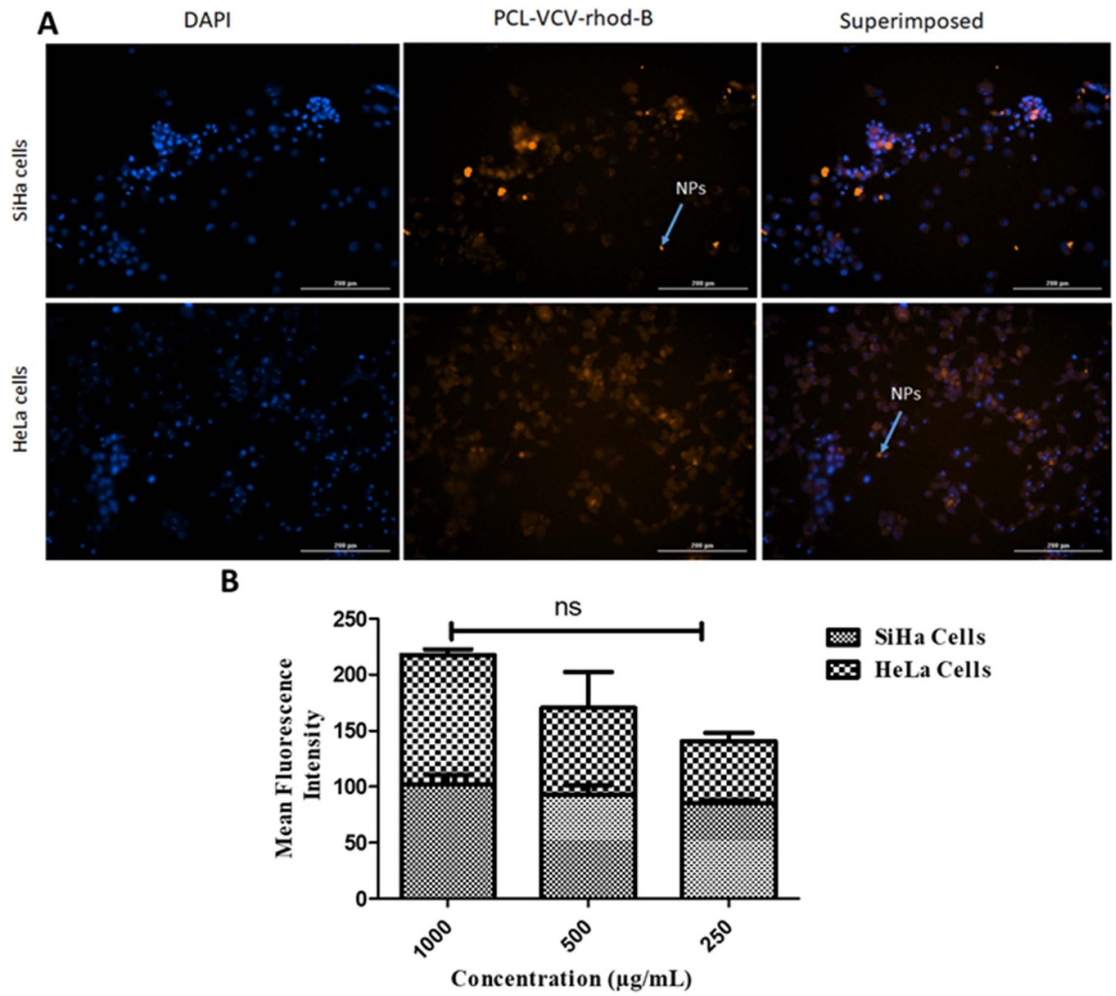

Figure 8. (A) Fluorescence microscope imaging of PCL-VCV-rhod-B uptake in HeLa and SiHa cell lines. The blue arrows show the localization of nanoparticles in the cells after 4 h of incubation. The nucleus is stained with DAPI (blue channel), and PCL-VCV-rhod-B labeled with rhodamine-B appear orange. (Scale bar: 200 µm). (B) Quantification of nanoparticle uptake at different concentrations in HeLa and SiHa cell lines. The data points in 8B are the mean ± standard deviation (n = 3) of the experiments. One-way ANOVA showed no significant difference in the cellular uptake of PCL-VCV-rhod-B between the highest and the lowest concentration in HeLa and SiHa cell lines ($p < 0.05$).

polymer matrix. These processes of improving the release profile of drug delivery system are well discussed in previously published articles [42, 43].

3.3. Cellular uptake assay

The intracellular uptake of PCL-VCV-rhod-B in different cell lines (HeLa and SiHa cells) was evaluated to determine the suitability of the NPs for targeted drug delivery. Both HeLa and SiHa cell lines (cervical carcinoma cell lines) were used because HSV-2 infection has been implicated as a risk factor for cervical carcinoma [44], and they are a reference model for understanding many biological processes, such as nanoparticle uptake and delivery [45]. The rate of nanoparticle uptake differed with the type of cell used [46]. However, Vero cells were used as standard HSV-2 hosts model to test for cytotoxicity and antiviral activity of nanoparticles because of their high susceptibility to HSV-2 infection and their ease of maintenance during cell culturing, providing insights into the virus's behavior and potential antiviral strategies. In addition, Vero cells were used for cytotoxicity assay to corroborate the data from the virus inhibition assay. Although the location of the nanoparticles uptake on the surface or within the cells is not well differentiated, it is however apparent that the nanoparticles are internalized close to the cell nucleus, suggesting that PCL-VCV-rhod-B are intracellularly located within the cells (figure 8(A)). Furthermore, the effect of nanoparticles concentration on cell uptake

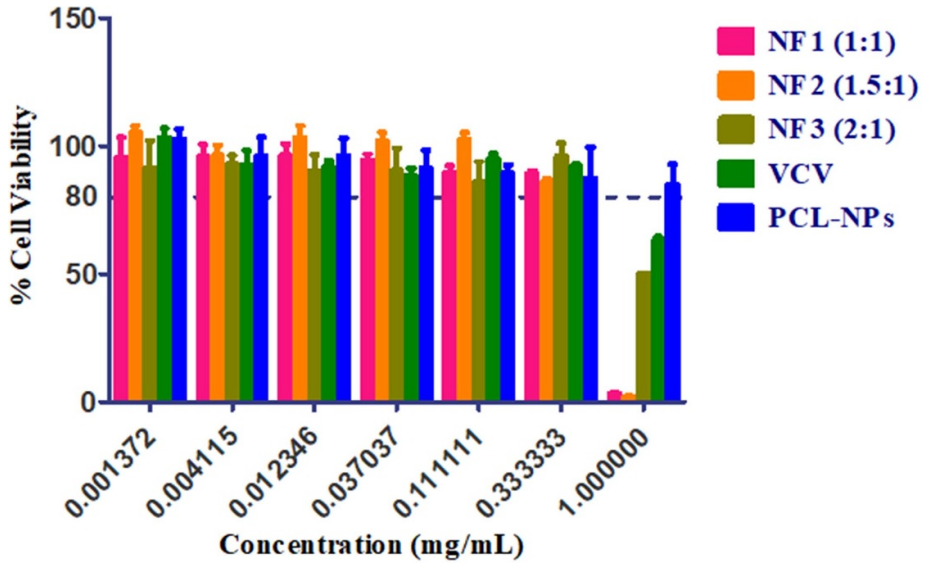

Figure 9. *In vitro* cell viability assay of VCV, drug-free NPs (PCL-NPs), NF1, NF2 and NF3 in Vero cells. PCL-VCV-NPs are categorized as NF1 (1:1), NF2 (1.5:1) and NF3 (2:1). The dotted line at the 80% mark shows the cell viability percentage where the assay is considered non-toxic. The data points are mean ± standard deviation (n = 3) of the experiments.

was determined. We discovered that as the concentration increased, the degree of the fluorescence emission in both SiHa and HeLa cells increased suggesting that the cells take up or internalize larger amounts of the nanoparticles (figure 8(B)).

3.4. Assessment of the cytotoxic effect of PCL-VCV-NPs on Vero cells

To determine the toxic effect of the nanoparticles and the free drug (VCV) on Vero cells, cell viability assay using MTT was conducted. Figure 9 shows the effect of the concentration of the test compounds (VCV, PCL-NPs, PCL-VCV-NPs) on the percentage cell viability of Vero cells. At a starting concentration of 1 mg ml^{-1}, all the test compounds showed signs of toxicity to Vero cells except PCL-NPs (drug-free nanoparticles). This further confirmed the non-toxicity of polycaprolactone (PCL) and its suitability for drug delivery [47]. The order of cell viability in this study is NF2 < NF1 < NF3 < VCV < PCL-NPs. All the test compounds were non-toxic to Vero cells at 0.3 mg ml^{-1}. At these concentrations, the cell viability of VCV and PCL-VCV-NPs were within the range of 85 ± 13.6%−100 ± 4.8%. The decrease in the percentage cell viability observed with PCL-VCV-NPs treated Vero cells may be attributed to the size of the nanoparticles [48], as small nanoparticles agglomerate quickly, influencing the interaction between the nanoparticles and the cells. The interaction between the agglomerated nanoparticles and the cells may hinder cell viability.

3.5. Evaluation of the anti-herpetic activities of VCV-loaded polymeric nanoparticles

The neutralization efficiency of PCL-VCV-NPs and PCL-NPs against HSV-2 infected Vero cells was determined and compared with the free drug (VCV). An effective treatment should induce an inhibitory effect against HSV-2, to prevent the virus from forming cytopathic effects on the cells (figure 10(C)). The neutralization efficiency of all the test compounds against HSV-2 infection in Vero cells are shown in figure 10. The result from the neutralization assay showed that PCL-NPs (nanoparticles without the drug) did not inhibit HSV-2 infection in Vero cells (figure 10(A)). PCL-VCV-NPs had a better neutralization efficiency than VCV. In this study, NF2 showed the highest neutralization effect against HSV-2 infection with an inhibition efficiency of 72%, NF3 showed 66% inhibition, NF1 inhibited HSV-2 infection by 62% while VCV showed 48% inhibition of HSV-2 infected cells. The half-maximal inhibitory concentration (IC_{50}) of PCL-VCV-NPs and VCV was evaluated to measure the efficacy of the drug and the drug loaded nanoparticles. The recorded IC_{50} values of NF1, NF2, NF3 and VCV are 0.1, 0.09, 0.1 and 0.12 mg ml^{-1} respectively (figure 10(B)). The improved antiviral potential of PCL-VCV-NPs against HSV-2 may be due to the changes observed in the physicochemical properties of the nanoparticles. The size (nanometer) and the shape of PCL-VCV-NPs also play a significant role in their improved antiviral activity. Nanoparticles with small sizes have a large surface area to volume ratio which increases their interaction with viral surfaces, entering the viral membrane to elicit antiviral activity. In addition, the spherical shape of PCL-VCV-NPs allowed the nanoparticles to interact directly with HSV-2. The shape of nanoparticles can affect their interaction with cellular receptors, influencing their ability to block virus binding and entry [49]. Despite the non-significant improvement observed with the use of

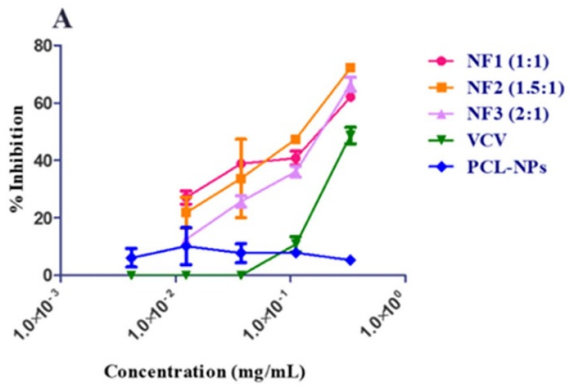

B

Virus	NF1	NF2	NF3	VCV
	(IC_{50} mg/mL)			
HSV-2	0.1	0.09	0.1	0.12
Fold increase ratio to VCV	1.2	1.3	1.2	NA
$p<0.05$	ns	ns	ns	

Figure 10. Anti-herpetic neutralization of PCL-VCV-NPs, PCL-NPs and VCV against HSV-2 infected Vero cells. (A) Antiviral inhibition of PCL-VCV-NPs at different drug to polymer ratios. (B) IC_{50} values of PCL-VCV-NPs (NF1, NF2, and NF3) against HSV-2 infected cells. (C) Microscopic illustration of Vero cells infected with HSV-2 live virus, uninfected and HSV-2 infected cells with PCL-VCV-NPs treatment. The blue arrows showed virus-induced cytopathic effect (cell rounding and cell aggregation) of HSV-2 on Vero cells. Data represents the mean ± SD of triplicate experiments.

PCL-VCV-NPs, this study serves as a proof-of-concept to test the efficacy of PCL-VCV-NPs against HSV-2 and the 1.2–1.3-fold increase in inhibition compared to the free drug is an indication that drug encapsulation plays a role in enhancing drug delivery and drug potency. PCL-VCV-NPs may still offer other advantages such as improved drug stability, enhanced biocompatibility, or targeted delivery. Further studies are necessary to improve the encapsulation method for more robust drug delivery and potency.

4. Conclusion

The risk of HSV-2 infection, combined with the virus's detrimental effects on the host, necessitates the development of alternative treatment options. This study successfully synthesized and characterized valacyclovir-loaded PCL nanoparticles, which were then used to treat HSV-2-infected Vero cells. The optimized physicochemical properties of valacyclovir-loaded PCL nanoparticles improved their antiviral activity against HSV-2 infected Vero cells when compared to the conventional drug, demonstrating the nanoparticles' potential as a more effective antiviral therapy. As much as this study showed PCL-VCV-NPs potential as an effective antiviral therapy, an improved delivery of the encapsulated drug may further enhance the effectiveness of the nanoparticles. Future research efforts should focus on evaluating the colloidal stability of the drug-bearing system in various suspension media and durations, with a focus on parameters such as particle size, ZP, and drug release patterns to ensure long-term stability and performance.

Data availability statement

The data that support the findings of this study are available upon reasonable request from the authors.

Funding

This research was supported by the National Research Foundation, South Africa, Grant No: 121936 and Reference Number PSTD23031683492.

Conflict of interest

All authors confirm that there is no competing interest to disclose.

Author contributions

O S O: Conceptualization, methodology, Investigation, data analysis, and writing-original draft. H T M: Conceptualization, methodology, supervision, and writing-original draft and editing. L L T: Methodology, supervision, data analysis, and editing. L N T: Supervision, methodology,

and editing. B R: Methodology and editing. M P N: Methodology and editing. S R: Methodology, Writing, analysis and editing.

Statement of Human and animal rights

No human and animal subjects were used by any of the authors in the study.

Consent for publication

All authors read and approved the final manuscript and agree with its publication.

ORCID iDs

Oluwafemi Samuel Obisesan https://orcid.org/0000-0003-2165-3636
Lesego Tshweu https://orcid.org/0000-0001-9480-7064
Bathabile Ramalapa https://orcid.org/0000-0002-9211-4990
Mpho Phehello Ngoepe https://orcid.org/0000-0001-7682-9489
Roux Saartjie https://orcid.org/0000-0002-6823-8934
Hazel Tumelo Mufhandu https://orcid.org/0000-0002-1551-3314

References

[1] WHO 2023 *Herpes Simplex Virus* (World Health Organisation)
[2] Orlowski P, Tomaszewska E, Gniadek M, Baska P, Nowakowska J, Sokolowska J, Nowak Z, Donten M, Celichowski G and Grobelny J 2014 Tannic acid modified silver nanoparticles show antiviral activity in herpes simplex virus type 2 infection *PLoS One* **9** e104113
[3] Galdiero S, Falanga A, Vitiello M, Cantisani M, Marra V and Galdiero M 2011 Silver nanoparticles as potential antiviral agents *Molecules* **16** 8894–918
[4] Shen M-X, Ma N, Li M-K, Liu Y-Y, Chen T, Wei F, Liu D-Y and Hou W Xiong H-R and Yang Z-Q 2019 Antiviral properties of R. tanguticum nanoparticles on herpes simplex virus type I in vitro and in vivo *Front. Pharmacol.* **10** 959
[5] Gaikwad S, Ingle A, Gade A, Rai M, Falanga A, Incoronato N, Russo L, Galdiero S and Galdiero M 2013 Antiviral activity of mycosynthesized silver nanoparticles against herpes simplex virus and human parainfluenza virus type 3 *Int. J. Nanomed.* **8** 4303–14
[6] Seyfizadeh N, Kalbermatter D, Imhof T, Ries M, Müller C, Jenner L, Blumenschein E, Yendrzheyevskiy A, Grün F and Moog K 2024 Development of a highly effective combination monoclonal antibody therapy against Herpes simplex virus *J. Biomed. Sci.* **31** 56
[7] Pradeep B, Nagamadhu M, Banji D, Madhavi B B, Arjun G and Shekhar K 2011 Formulation and evaluation of valacyclovir hydrochloride microcapsules *Int. J. Pharm. Pharm. Sci.* **3** 92–96
[8] Shenoy V 2020 *A Proteomic Approach to Identification of Prodrug-Activating Serine Hydrolases* (Activation of Valacyclovir)
[9] Pundkar A S and Arsul V A 2018 Analytical method development and validation of valacylovir hydrochloride by uv and hplc
[10] Zhang S, Zheng M, Zhou M, Chen T, Wang N, Zhang Z and Zhang G 2017 A new hemihydrate of valacyclovir hydrochloride *Crystals* **7** 140
[11] Bukhari S, Aslam H M, Awwal T A, Christmas D and Wallach S L 2020 Valacyclovir-induced thrombotic thrombocytopenic purpura *Cureus* **12** 5
[12] Haleem A, Javaid M, Singh R P, Rab S and Suman R 2023 Applications of nanotechnology in medical field *Glob. Health J.* **7** 70–77
[13] Patra J K, Das G, Fraceto L F, Campos E V R, Rodriguez-Torres M D P, Acosta-Torres L S, Diaz-Torres L A, Grillo R, Swamy M K and Sharma S 2018 Nano based drug delivery systems: recent developments and future prospects *J. Nanobiotechnol.* **16** 1–33
[14] Yusuf A, Almotairy A R Z, Henidi H, Alshehri O Y and Aldughaim M S 2023 Nanoparticles as drug delivery systems: a review of the implication of nanoparticles' physicochemical properties on responses in biological systems *Polymers* **15** 1596
[15] Jeevanandam J, San Chan Y and Danquah M K 2016 Nano-formulations of drugs: recent developments, impact and challenges *Biochimie* **128** 99–112
[16] Charelli L E, de Mattos G C, de Jesus Sousa-batista A, Pinto J C and Balbino T A 2022 Polymeric nanoparticles as therapeutic agents against coronavirus disease *J. Nanoparticle Res.* **24** 1–15
[17] Singh L, Kruger H G, Maguire G E, Govender T and Parboosing R 2017 The role of nanotechnology in the treatment of viral infections *Ther. Adv. Infect. Dis.* **4** 105–31
[18] Kirtane A R, Verma M, Karandikar P, Furin J, Langer R and Traverso G 2021 Nanotechnology approaches for global infectious diseases *Nat. Nanotechnol.* **16** 369–84
[19] Aguilera-Correa J J, Esteban J and Vallet-Regí M 2021 Inorganic and polymeric nanoparticles for human viral and bacterial infections prevention and treatment *Nanomaterials* **11** 137
[20] Lima T L C et al 2018 Improving encapsulation of hydrophilic chloroquine diphosphate into biodegradable nanoparticles: a promising approach against herpes virus simplex-1 infection *Pharmaceutics* **10** 255
[21] Reed L J and Muench H 1938 A simple method of estimating fifty per cent endpoints *Am. J. Epidemiol.* **27** 493–7
[22] Zhu Y-H, Wang J-L, Zhang H-B, Khan M I, Du X-J and Wang J 2019 Incorporation of a rhodamine B conjugated polymer for nanoparticle trafficking both in vitro and in vivo *Biomater. Sci.* **7** 1933–9
[23] Obisesan O S, Tshweu L L, Chauke S, Malatji K B, Ramalapa B, Alexandre K B and Mufhandu H T 2024 Synthesis and characterization of tenofovir disoproxil fumarate loaded nanoparticles for HIV-1 treatment *Nano Select* **5** 2300157
[24] Orasugh J T, Saha N R, Rana D, Sarkar G, Mollick M M R, Chattoapadhyay A, Mitra B C, Mondal D, Ghosh S K and Chattopadhyay D 2018 Jute cellulose nano-fibrils/hydroxypropylmethylcellulose nanocomposite: a novel material with potential for application in packaging and transdermal drug delivery system *Ind Crops Prod.* **112** 633–43
[25] Mufhandu H T, Obisesan O S, Ajiboye T O, Mhlanga S D and Onwudiwe D C 2023 Antiviral potential of selected N-methyl-N-phenyl dithiocarbamate complexes against human immunodeficiency virus (HIV) *Microbiol. Res.* **14** 355–70
[26] Wang M, Jiang S, Zhou L, Wang C, Mao R and Ponnusamy M 2017 Efficient production of recombinant glycoprotein D of herpes simplex virus type 2 in Pichia pastoris and its protective efficacy against viral challenge in mice *Arch. Virol.* **162** 701–11
[27] Huang W, Tsui C P, Tang C Y and Gu L 2018 Effects of compositional tailoring on drug delivery behaviours of silica xerogel/polymer core-shell composite nanoparticles *Sci. Rep.* **8** 13002

[28] Sánchez A, Mejía S P and Orozco J 2020 Recent advances in polymeric nanoparticle-encapsulated drugs against intracellular infections *Molecules* **25** 3760
[29] Shang L, Nienhaus K and Nienhaus G U 2014 Engineered nanoparticles interacting with cells: size matters *J. Nanobiotechnol.* **12** 1–11
[30] Yuan T, Gao L, Zhan W and Dini D 2022 Effect of particle size and surface charge on nanoparticles diffusion in the brain white matter *Pharm. Res.* **39** 767–81
[31] Adabi M, Naghibzadeh M, Adabi M, Zarrinfard M A, Esnaashari S S, Seifalian A M, Faridi-Majidi R, Tanimowo Aiyelabegan H and Ghanbari H 2017 Biocompatibility and nanostructured materials: applications in nanomedicine *Artif. Cells Nanomed. Biotechnol.* **45** 833–42
[32] Moore T L, Rodriguez-Lorenzo L, Hirsch V, Balog S, Urban D, Jud C, Rothen-Rutishauser B, Lattuada M and Petri-Fink A 2015 Nanoparticle colloidal stability in cell culture media and impact on cellular interactions *Chem. Soc. Rev.* **44** 6287–305
[33] Kladko D V, Falchevskaya A S, Serov N S and Prilepskii A Y 2021 Nanomaterial shape influence on cell behavior *Int. J. Mol. Sci.* **22** 5266
[34] Fornaguera C and Solans C 2018 Analytical methods to characterize and purify polymeric nanoparticles *Int. J. Polym. Sci.* **2018** 1–10
[35] Wu Y F, Zhang H, Wang N X, Chen T and Liu Y 2021 A study on the crystal transformation relationships of valacyclovir hydrochloride polymorphs: sesquihydrate, form I, and form II *Cryst. Res. Technol.* **56** 2100084
[36] Padsalgikar A 2017 *Plastics in Medical Devices for Cardiovascular Applications* (William Andrew)
[37] Pandurangappa M and Kumar K S 2011 Micellar mediated trace level mercury quantification through the rhodamine B hydrazide spirolactam ring opening process *Anal. Methods* **3** 715–23
[38] Kerman I, Toppare L, Yilmaz F and Yagci Y 2005 Thiophene ended ϵ-caprolactone conducting copolymers and their electrochromic properties *J. Macromol. Sci. A* **42** 509–20
[39] De R, Mahata M K and Kim K T 2022 Structure-based varieties of polymeric nanocarriers and influences of their physicochemical properties on drug delivery profiles *Adv. Sci.* **9** 2105373
[40] Herdiana Y, Wathoni N, Shamsuddin S and Muchtaridi M 2021 Drug release study of the chitosan-based nanoparticles *Heliyon* **8** e08674
[41] Surya Teja S, Mothilal M, Damodharan N and Jaison D 2018 Screening and optimization of valacyclovir niosomes by design of experiments *Int. J. Appl. Pharm.* **10** 79–85
[42] Chaerunisaa A Y, Ali R, Körber M and Bodmeier R 2020 Quantification of porogen effect on the drug release from single-and multi-layered ethylcellulose coated pellets containing single or combined drugs *Int. J. Pharm.* **577** 119050
[43] Ghasemiyeh P and Mohammadi-Samani S 2021 Polymers blending as release modulating tool in drug delivery *Front. Mater.* **8** 752813
[44] Sausen D G, Shechter O, Gallo E S, Dahari H and Borenstein R 2023 Herpes simplex virus, human papillomavirus, and cervical cancer: overview, relationship, and treatment implications *Cancers* **15** 3692
[45] Behzadi S, Serpooshan V, Tao W, Hamaly M A, Alkawareek M Y, Dreaden E C, Brown D, Alkilany A M, Farokhzad O C and Mahmoudi M 2017 Cellular uptake of nanoparticles: journey inside the cell *Chem. Soc. Rev.* **46** 4218–44
[46] Shin H, Kwak M, Lee T G and Lee J Y 2020 Quantifying the level of nanoparticle uptake in mammalian cells using flow cytometry *Nanoscale* **12** 15743–51
[47] Pawar R, Pathan A, Nagaraj S, Kapare H, Giram P and Wavhale R 2023 Polycaprolactone and its derivatives for drug delivery *Polym. Adv. Technol.* **34** 3296–316
[48] Bao Y, Maeki M, Ishida A, Tani H and Tokeshi M 2022 Effect of organic solvents on a production of PLGA-based drug-loaded nanoparticles using a microfluidic device *ACS Omega* **7** 33079–86
[49] Maginnis M S 2018 Virus–receptor interactions: the key to cellular invasion *J. Mol. Biol.* **430** 2590–611